JLAB-THY-03-199
WM-03-110

Higher moments of nucleon spin structure functions in heavy baryon chiral perturbation theory and in a resonance model

Chung-Wen Kao
Department of Physics and Astronomy,
University of Manchester, Manchester, M13 9PL UK *

D. Drechsel, S. Kamalov
Institut für Kernphysik, Johannes Gutenberg-Universität, D-55099 Mainz, Germany

M. Vanderhaeghen
Department of Physics, College of William and Mary,
Williamsburg, VA 23187, USA and
Jefferson Laboratory, Newport News, VA 23606, USA

(Dated: 11th March 2009)

Abstract

The third moment d_2 of the twist-3 part of the nucleon spin structure function g_2 is generalized to arbitrary momentum transfer Q^2 and is evaluated in heavy baryon chiral perturbation theory (HBChPT) up to order $\mathcal{O}(p^4)$ and in a unitary isobar model (MAID). We show how to link d_2 as well as higher moments of the nucleon spin structure functions g_1 and g_2 to nucleon spin polarizabilities. We compare our results with the most recent experimental data, and find a good description of these available data within the unitary isobar model. We proceed to extract the twist-4 matrix element f_2 which appears in the $1/Q^2$ suppressed term in the twist expansion of the spin structure function g_1 for proton and neutron.

PACS numbers: 11.55.Hx, 13.60.Hb, 14.20.Dh

* Present address : Department of Physics, North Carolina State University, Raleigh, NC 27695 - 8202, USA

I. INTRODUCTION

The forward scattering of spacelike virtual photons (with virtuality Q^2) on the nucleon, allows one to study sum rules which relate nucleon structure quantities to inclusive electroproduction cross sections. At large Q^2, it yields the sum rules studied in deep-inelastic scattering (DIS) experiments (see Ref. [1] for a recent review). The study of such sum rules as function of Q^2 from the real photon point to large Q^2, opens up the perspective to interpolate between the non-perturbative and perturbative regimes of QCD, as one goes from low to high Q^2.

The moment d_2 of the nucleon spin structure functions can be measured by scattering longitudinally polarized electron beams off nucleon targets with transverse and longitudinal polarizations. Being a higher moment in the Bjorken variable x, d_2 contains appreciable contributions from the resonance region. It is therefore the aim of this letter to study the threshold and resonance contributions to d_2 within the frameworks of heavy baryon chiral perturbation theory (HBChPT) and of a unitary isobar model (MAID).

Since a measurement of d_2 requires also transverse polarization, experimental information on this observable has become available only recently at SLAC [2, 3] and JLab [4]. Further experiments are underway or proposed at JLab [Mez03]. In particular, the SLAC experiments [3] yielded the values : $d_2^p = 0.0032 \pm 0.0017$ and $d_2^n = 0.0079 \pm 0.0048$ at $Q^2 = 5$ GeV^2.

At large momentum transfers, a non-zero value for d_2 directly measures a twist-3 quark-gluon matrix element in the nucleon, which has been estimated within several model calculations as well as within lattice QCD. In this paper, we show that when generalizing the definition of d_2 to arbitrary momentum transfers, its physical interpretation can be expressed in terms of generalized (i.e. Q^2 dependent) spin polarizabilities of the nucleon. These generalized polarizabilities appear in the analysis of the forward virtual Compton scattering amplitude (for a review, see Ref. [6]). Using the calculation of these spin polarizabilities within HBChPT [7] (see also Refs. [8, 9]), and within a unitary isobar model [10], we evaluate d_2. In an analogous way, the third moment of the spin structure function g_1 can be expressed through these spin polarizabilities. These generalized definitions for d_2 and the third moment of g_1 constitute useful observables to interpolate between a hadronic description at low Q^2 and a partonic description, based on the Operator Product Expansion (OPE) at large Q^2.

Besides the twist-3 matrix element d_2, the $1/Q^2$ suppressed term in the twist expansion of the first moment of g_1 also contains the twist-4 matrix element f_2. It has been suggested (see e.g. Ref.[1]) that the matrix elements d_2 and f_2 enter in the response of the color electric and magnetic fields to the polarization of the nucleon in its rest frame, which can be expressed in terms of gluon field polarizabilities. Therefore an extraction of f_2, besides d_2, can yield us interesting new nucleon structure information. Such an phenomenological extraction was peformed for the first time in Ref. [11] based on the SLAC data of Ref. [2]. With the advent of the recent JLab data for the first moment of the proton and neutron spin structure function g_1 in the intermediate Q^2 range, we may now perform a phenomenological analysis based on all available data to extract the twist-4 matrix element f_2.

The outline of the paper is as follows. In Section II, we review the twist expansion of the moments of the nucleon spin structure functions g_1 and g_2 and show how the definitions for the third moments of the nucleon structure functions g_1 and g_2 can be generalized at arbitrary Q^2 in terms of nucleon spin polarizabilities.

In Section III, we use the calculation of these spin polarizabilities within HBChPT to evaluate d_2 and the third moments of g_1 and g_2.

In Section IV, we show how these observables can be expressed in multipoles which arise naturally when performing an evaluation within an isobar model.

In Section V, we show our results for d_2 and the third moments of g_1 and g_2 within both ChPT and a unitary isobar model and compare with recent experimental data for d_2. We also compare our results for the first moment of g_1 with the available data for both proton and neutron and use the twist-expansion for the first moment of g_1 to extract the magnitude of the twist-4 matrix element f_2.

Finally, we give our conclusions in Section VI.

II. TWIST EXPANSION AND MOMENTS OF NUCLEON SPIN STRUCTURE FUNCTIONS

At sufficiently large momentum transfer $Q^2 >> \Lambda^2_{QCD}$, one can perform a twist expansion for the moments of the nucleon structure functions. We will consider in this work the

moments of the nucleon spin structure functions g_1 and g_2, which are defined as :

$$\Gamma_1^{(n)}(Q^2) \equiv \int_0^1 dx\, x^{n-1}\, g_1(x,\, Q^2)\,, \qquad n = 1, 3, 5, ... \tag{1}$$

$$\Gamma_2^{(n)}(Q^2) \equiv \int_0^1 dx\, x^{n-1}\, g_2(x,\, Q^2)\,, \qquad n = 1, 3, 5, ... \tag{2}$$

In particular, for the first moment $\Gamma_1^{(1)}$ of g_1 such a twist expansion can be written as [13, 14] :

$$\Gamma_1^{(1)}(Q^2) = \Gamma_{1,\,tw-2}^{(1)}(Q^2) + \frac{M_N^2}{9\,Q^2}\left(a_2(Q^2) + 4d_2(Q^2) + 4f_2(Q^2)\right) + \mathcal{O}(\frac{M_N^4}{Q^4})\,. \tag{3}$$

The remaining Q^2 dependence in the coefficients $\Gamma_{1,\,tw-2}^{(1)}$, a_2, d_2 and f_2 of the twist expansion is logarithmic. In particular, the three-loop result for the leading (i.e. twist-2) term $\Gamma_{1,\,tw-2}^{(1)}(Q^2)$ is given, for 3 quark flavors, as [15, 16, 17] :

$$\begin{aligned}
&\Gamma_{1,\,tw-2}^{(1)}(Q^2) \\
&= \left[1 - \left(\frac{\alpha_s(Q^2)}{\pi}\right) - 3.5833\left(\frac{\alpha_s(Q^2)}{\pi}\right)^2 - 20.2153\left(\frac{\alpha_s(Q^2)}{\pi}\right)^3\right]\left(\pm\frac{1}{12}g_A + \frac{1}{36}a_8\right) \\
&+ \left[1 - 0.33333\left(\frac{\alpha_s(Q^2)}{\pi}\right) - 0.54959\left(\frac{\alpha_s(Q^2)}{\pi}\right)^2 - 4.44725\left(\frac{\alpha_s(Q^2)}{\pi}\right)^3\right]\frac{1}{9}\,a_0^\infty\,,
\end{aligned} \tag{4}$$

where in the term proportional to g_A the sign + (-) corresponds with proton (neutron) respectively, g_A is known from neutron beta decay, and a_8 is extracted from hyperon weak decay data assuming $SU(3)$ symmetry. The updated values for g_A [18] and a_8 [19] are given by :

$$g_A = 1.267 \pm 0.003\,, \tag{5}$$

$$a_8 = 0.585 \pm 0.023\,. \tag{6}$$

Furthermore, in Eq. (4), $a_0^\infty \equiv a_0(Q^2 = \infty)$ is the flavor singlet axial charge, which is fixed by measuring the first moment $\Gamma_1^{(1)}$ at a sufficiently large scale.

The $1/Q^2$ suppressed terms in Eq. (3) are of three different natures. The term proportional to $a_2(Q^2)$ arises due to target mass corrections and is given by the twist-2 part of the third moment of g_1 :

$$a_2(Q^2) \equiv 2\,\Gamma_{1,\,tw-2}^{(3)}(Q^2)\,. \tag{7}$$

The terms proportional to d_2 and f_2 in Eq. (3) correspond with dynamical higher-twist

corrections. The function d_2 corresponds with the matrix element of a twist-3 quark gluon operator, and can be expressed in terms of the twist-3 part of the spin structure function g_2 as :

$$d_2(Q^2) \;\equiv\; 3 \int_0^1 dx\, x^2 \left(g_2\,(x,\, Q^2) - g_2^{WW}(x,\, Q^2) \right) , \tag{8}$$

where g_2^{WW} is the twist-2 (Wandzura-Wilczek) part of g_2 [20]. Using the Wandzura-Wilczek relation, one can express Eq. (8) as :

$$d_2(Q^2) \;=\; \int_0^1 dx\, x^2 \left(3\, g_2\,(x,\, Q^2) + 2\, g_1(x,\, Q^2) \right) . \tag{9}$$

Several model estimates as well as lattice QCD calculations [22] have been performed for the twist-3 matrix element d_2. In particular, an estimate in the instanton vacuum approach [21], where d_2 is parametrically suppressed due to the diluteness of the instanton medium, predicted d_2 to be of order 10^{-3}. Also a revised lattice calculation [22] supports this small value. Such a small value for d_2, of order 10^{-3}, is in agreement with the recent experimental results from SLAC [3].

The function f_2 in Eq. (3) corresponds with the matrix element of a twist-4 quark gluon operator. Unlike a_2 and d_2, the matrix element f_2 cannot be expressed directly in terms of moments of g_1 and g_2 as in Eqs. (7) and (9). It can however be extracted phenomenologically from the twist expansion of Eq. (3) as :

$$\frac{4M_N^2}{9Q^2}\, f_2(Q^2) \equiv \left[\Gamma_1^{(1)}(Q^2) - \Gamma_{1,\,tw-2}^{(1)}(Q^2) \right] \;-\; \frac{M_N^2}{9Q^2} \left[a_2(Q^2) + 4d_2(Q^2) \right] , \tag{10}$$

by using the experimental information on the full Q^2 dependence of $\Gamma_1^{(1)}$ and provided one knows the twist-2 and twist-3 contributions $\Gamma_{1,\,tw-2}^{(1)}$, a_2 and d_2. In this way, f_2 has been estimated in Refs. [11, 12] for $Q^2 \gtrsim 0.5$ GeV^2 where the twist expansion was assumed to hold. Several model calculations have also been given for f_2, e.g. in the framework of the instanton vacuum approach [21] and using QCD sum rules [23], to which we refer further on.

Although the Operator Product Expansion (OPE) of Eq. (3) is only defined for $Q^2 >> \Lambda_{QCD}^2$, Eq. (9) can be used to define d_2 outside this range by keeping the full Q^2 dependence in the structure functions which appear in the integrand. Analogously, we can study the Q^2 dependence of the higher moments of g_1, such as $\Gamma_1^{(3)}(Q^2)$, outside the range of validity of the OPE. We next show that at low Q^2, the physical meaning of d_2 and $\Gamma_1^{(3)}$ can be

expressed in terms of nucleon polarizabilities which will be calculated in this work within Chiral Perturbation Theory and estimated within a phenomenological resonance approach. At large Q^2, d_2 and $\Gamma_1^{(3)}$ tend into the matrix elements appearing in the twist expansion of Eq. (3) and display only a logarithmic Q^2 dependence. Defined in this way, d_2 and $\Gamma_1^{(3)}$ are useful observables to interpolate between a hadronic description at low Q^2, involving the polarizabilities of the system, and a partonic description based on the OPE at large Q^2.

Starting with d_2, one can split the integral of Eq. (9) into an elastic contribution at $x = 1$ and an inelastic contribution. The elastic contribution is given by :

$$d_2^{el}(Q^2) \;=\; \left(G_E(Q^2) \,+\, \frac{G_E(Q^2) - G_M(Q^2)}{2(1 + 4M_N^2/Q^2)} \right) G_M(Q^2). \tag{11}$$

While this contribution vanishes like Q^{-8} for $Q^2 \to \infty$, it increases with smaller values of Q^2 and approaches $d_2^{\rm el}(0) = G_E(0) \,\cdot\, G_M(0)$. The inelastic contribution to d_2 corresponds with the integral over the excitation spectrum :

$$d_2^{inel}(Q^2) \;=\; \int_0^{x_0} dx \, x^2 \, \Big(3\, g_2\,(x,\, Q^2) + 2\, g_1(x,\, Q^2) \Big) \;. \tag{12}$$

where $x_0 = Q^2/(2M_N m_\pi + m_\pi^2 + Q^2)$ is the threshold for pion production.

To evaluate Eq. (12), we can equivalently express the third moment of the twist-3 part of g_2 in terms of the spin-dependent doubly virtual Compton scattering amplitude in the forward direction (VVCS). Following the notations of Refs. [6, 7], we use the VVCS amplitudes $g_{TT}(\nu, Q^2)$ and $g_{LT}(\nu, Q^2)$, where ν is the lab energy and Q^2 the virtuality of the virtual photon, and T (L) denotes the transverse (longitudinal) virtual photon polarization.

The imaginary parts of g_{TT} and g_{LT} are related to the virtual photon absorption cross sections σ_{TT} and σ_{LT}, multiplied by a photon flux factor K (with dimension of energy) [50]. These partial cross sections are related to the nucleon structure functions g_1 and g_2 as :

$$K \cdot \sigma_{TT} \;=\; \frac{4\pi^2 \alpha_{em}}{M_N} \Big(g_1(x, Q^2) - \gamma^2 g_2(x, Q^2) \Big), \tag{13}$$

$$K \cdot \sigma_{LT} \;=\; \frac{4\pi^2 \alpha_{em}}{M_N} \gamma \Big(g_1(x, Q^2) + g_2(x, Q^2) \Big)\,, \tag{14}$$

with $\gamma \equiv Q/\nu$ and $x \equiv Q^2/(2M_N\,\nu)$.

For the non-pole (i.e. *inelastic*) contributions to g_{TT} and g_{LT}, one can perform a low energy expansion (LEX) as follows [6] :

$$\mathrm{Re}\; g_{TT}(\nu,\, Q^2) \,-\, \mathrm{Re}\; g_{TT}^{\rm pole}(\nu,\, Q^2) \,=\, \left(\frac{2\,\alpha_{\rm em}}{M_N^2} \right) I_A(Q^2)\,\nu \,+\, \gamma_0(Q^2)\,\nu^3 \,+\, \mathcal{O}(\nu^5)\,, \tag{15}$$

$$\text{Re}\; g_{LT}(\nu,\,Q^2) - \text{Re}\; g_{LT}^{\text{pole}}(\nu,\,Q^2) \;=\; \left(\frac{2\,\alpha_{\text{em}}}{M_N^2}\right) Q\, I_3(Q^2) \,+\, Q\,\delta_{LT}(Q^2)\,\nu^2 \,+\, \mathcal{O}(\nu^4)\,. \tag{16}$$

For the $\mathcal{O}(\nu)$ term in Eq. (15), one obtains a generalization of the GDH sum rule as :

$$\begin{aligned} I_A(Q^2) \;&=\; \frac{M_N^2}{4\,\pi^2\,\alpha_{\text{em}}} \int_{\nu_0}^{\infty} \frac{K(\nu,\,Q^2)}{\nu}\,\frac{\sigma_{TT}\,(\nu,\,Q^2)}{\nu}\,d\nu\,, \\ &=\; \frac{2\,M_N^2}{Q^2}\int_0^{x_0} dx\,\left\{g_1\,(x,\,Q^2) \,-\, \frac{4M_N^2}{Q^2}\,x^2\,g_2\,(x,\,Q^2)\right\}\,, \end{aligned} \tag{17}$$

and recovers the GDH sum rule at $Q^2 = 0$, as $I_A(0) = -\kappa_N^2/4$, with κ_N the nucleon anomalous magnetic moment ($\kappa_p = 1.79$, $\kappa_n = -1.91$).

Furthermore we introduce the integral I_1, which is related to the inelastic part of the first moment $\Gamma_1^{(1)}$ of g_1 as :

$$I_1(Q^2) \;=\; \frac{2\,M_N^2}{Q^2}\int_0^{x_0} dx\,g_1\,(x,\,Q^2)\,, \tag{18}$$

and which also approaches the GDH value at $Q^2 = 0$.

The higher order terms in Eqs. (15) and (16) can be expressed in terms of nucleon spin polarizabilities, see Ref. [6]. In particular, the $\mathcal{O}(\nu^2)$ term in g_{LT} is given by :

$$\begin{aligned} \delta_{LT}\,(Q^2) \;&=\; \frac{1}{2\pi^2}\int_{\nu_0}^{\infty} \frac{K(\nu,\,Q^2)}{\nu}\,\frac{\sigma_{LT}(\nu\,Q^2)}{Q\,\nu^2}\,d\nu\,, \\ &=\; \frac{\alpha_{\text{em}}\,16\,M_N^2}{Q^6}\int_0^{x_0} dx\,x^2\,\left\{g_1\,(x,\,Q^2) \,+\, g_2\,(x,\,Q^2)\right\}\,. \end{aligned} \tag{19}$$

Combining Eqs. (17,18,19), we find that the inelastic contribution to the third moment d_2 of Eq. (12) can be expressed as :

$$d_2^{inel}(Q^2) \;=\; \frac{Q^6}{8M_N^2}\left\{-\frac{1}{M_N^2\,Q^2}\left(I_A(Q^2) - I_1(Q^2)\right) \,+\, \frac{1}{\alpha_{\text{em}}}\,\delta_{LT}(Q^2)\right\}\,. \tag{20}$$

We can perform a similar analysis for the moments $\Gamma_1^{(n)}$ and $\Gamma_2^{(n)}$ defined through Eqs. (1) and (2). The elastic contribution to $\Gamma_1^{(n)}$ is given by :

$$\Gamma_1^{(n)\,el}(Q^2) \;=\; \frac{1}{2}\,\frac{1}{1 + Q^2/(4M_N^2)}\left(G_E(Q^2) \,+\, \frac{Q^2}{4M_N^2}\,G_M(Q^2)\right) G_M(Q^2). \tag{21}$$

While this contribution vanishes like Q^{-8} for $Q^2 \to \infty$, it approaches $\Gamma_1^{(n)\,el}(0) = 1/2 \cdot G_E(0) \cdot G_M(0)$ at the real photon point. The inelastic contribution to $\Gamma_1^{(n)}$ corresponds with the integral over the excitation spectrum :

$$\Gamma_1^{(n)\,inel}(Q^2) \;=\; \int_0^{x_0} dx\,x^{n-1}\,g_1(x,\,Q^2)\,. \tag{22}$$

The third moment $\Gamma_1^{(3)\,inel}$ can be expressed in terms of the quantities introduced in Eqs. (17,18,19) as :

$$\Gamma_1^{(3)\,inel}(Q^2) \;=\; \frac{Q^6}{8M_N^2}\left\{\frac{1}{M_N^2\,Q^2}\left(I_A(Q^2) - I_1(Q^2)\right) \;+\; \frac{1}{2\,\alpha_{\rm em}}\,\delta_{LT}(Q^2)\right\}. \qquad (23)$$

For $\Gamma_2^{(n)}$, the elastic contribution is given by :

$$\Gamma_2^{(n)\,el}(Q^2) \;=\; -\frac{1}{2}\,\frac{Q^2}{4M_N^2 + Q^2}\left(G_M(Q^2) \,-\, G_E(Q^2)\right)\,G_M(Q^2). \qquad (24)$$

This contribution vanishes at the real photon point. The inelastic contribution to $\Gamma_2^{(n)}$ corresponds with the integral over the excitation spectrum :

$$\Gamma_2^{(n)\,inel}(Q^2) \;=\; \int_0^{x_0} dx\, x^{n-1}\, g_2(x,\,Q^2)\,. \qquad (25)$$

The third moment $\Gamma_2^{(3)\,inel}$ can be expressed in terms of the quantities introduced in Eqs. (17,18) as :

$$\Gamma_2^{(3)\,inel}(Q^2) \;=\; -\frac{Q^4}{8M_N^4}\left(I_A(Q^2) - I_1(Q^2)\right). \qquad (26)$$

Note that $\Gamma_2^{(3)}$ is linearly dependent on d_2 and $\Gamma_1^{(3)}$ as it can be expressed as :

$$\Gamma_2^{(3)}(Q^2) \;=\; \frac{1}{3}\left(d_2(Q^2) - 2\,\Gamma_1^{(3)}(Q^2)\right). \qquad (27)$$

Although we restrict our investigation in this work up to the third moment of g_1 and g_2, one can in principle extend the analysis to the higher moments $\Gamma_1^{(n)}$ and $\Gamma_2^{(n)}$, with $n = 5, 7 ...$. Their expressions involve higher spin polarizabilities, as have e.g. been introduced at the real photon point in Ref. [25].

III. CALCULATION OF THE MOMENTS d_2, $\Gamma_1^{(3)}$, AND $\Gamma_2^{(3)}$ IN HBChPT

Eqs. (20,23,26) show that $d_2^{inel}(Q^2)$, $\Gamma_1^{(3)\,inel}(Q^2)$ and $\Gamma_2^{(3)\,inel}(Q^2)$ can be expressed in terms of I_A, I_1 and δ_{LT} appearing in a low energy expansion of the forward VVCS amplitudes . These expressions have been calculated at low Q^2 in HBChPT, which allow us to construct the HBChPT predictions for d_2^{inel}, $\Gamma_1^{(3)\,inel}$ and $\Gamma_2^{(3)\,inel}$. The expressions for I_A and I_1 in HBChPT have been obtained up to $\mathcal{O}(p^4)$ in Refs. [26, 27] :

$$I_1(Q^2) \;=\; -\frac{1}{16}[(\kappa_s + \kappa_v\tau_3)^2]$$

$$
\begin{aligned}
& + \frac{g_A^2 M_N^2}{(4\pi F_\pi)^2} \cdot \frac{m_\pi}{M_N} \cdot \frac{\pi}{32}\{(-10-12\kappa_v)+(-2-12\kappa_s)\tau_3 \\
& \qquad + [(20+24\kappa_v)+(4+24\kappa_s)\tau_3]\cdot\frac{1}{w}\tan^{-1}[\frac{w}{2}] \\
& \qquad + [(3+6\kappa_v)+(3+10\kappa_s)\tau_3]\cdot w\tan^{-1}[\frac{w}{2}]\}, \qquad (28)
\end{aligned}
$$

$$
\begin{aligned}
I_A(Q^2) &= -\frac{1}{16}[(\kappa_s+\kappa_v\tau_3)^2] \\
&+ \frac{g_A^2 M_N^2}{(4\pi F_\pi)^2}\, 2\left(\frac{\sqrt{w^2+4}}{w}\sinh^{-1}[\frac{w}{2}] - 1\right) \\
&- \frac{g_A^2 M_N^2}{(4\pi F_\pi)^2} \cdot \frac{m_\pi}{M_N} \cdot \frac{\pi}{16}\{(-10-2\kappa_v+8w^2)+(-2+6\kappa_s)\tau_3 \\
& \qquad + [(20+4\kappa_v)+(4-12\kappa_s)\tau_3]\cdot\frac{1}{w}\tan^{-1}[\frac{w}{2}] \\
& \qquad + [(3+3\kappa_v)+(3-\kappa_s)\tau_3]\cdot w\tan^{-1}[\frac{w}{2}]\}, \qquad (29)
\end{aligned}
$$

with $w = \sqrt{\frac{Q^2}{m_\pi^2}}$. These expressions are given in terms of the renormalized isoscalar (κ_s) and isovector (κ_v) anomalous magnetic moments, whose physical values are given by $\kappa_s = -0.12$ and $\kappa_v = 3.70$. Furthermore, throughout this paper we use the values $g_A = 1.267$, $F_\pi = 0.0924$ GeV, and $m_\pi = 0.14$ GeV. While both I_1 of Eq. (28) and I_A of Eq. (29) approach the GDH value of $-\kappa_N^2/$ at $Q^2 = 0$, their slopes at this point differe substantially : $I_1^{'}(0) = (6.31 + 0.66\ \tau_3)$ / GeV^2 and $I_A^{'}(0) =$ - $(12.43 + 2.09\ \tau_3)$ / GeV^2.

The longitudinal-transverse generalized forward spin polarizability δ_{LT} of Eq. (16) has also been calculated in HBChPT [7] (see Ref. [9] for the corresponding calculation within the framework of relativistic baryon ChPT). For the $\mathcal{O}(p^3)$ term, the result is :

$$
\delta_{LT}^{\mathcal{O}(p^3)}(Q^2) = \frac{\alpha_{em} g_A^2}{(4\pi F_\pi)^2} \cdot \frac{4}{m_\pi^2}\left[\frac{1}{3w\sqrt{w^2+4}}\sinh^{-1}[\frac{w}{2}]\right], \qquad (30)
$$

and the $\mathcal{O}(p^4)$ correction is given by :

$$
\begin{aligned}
\delta_{LT}^{\mathcal{O}(p^4)}(Q^2) = \frac{\alpha_{em} g_A^2}{(4\pi F_\pi)^2 m_\pi^2} \cdot \frac{m_\pi}{M_N} \cdot \frac{\pi}{64} \quad & \{(-16+8\kappa_v)+(-8+16\kappa_s)\tau_3 \\
& + [(-54+8\kappa_v)+(-6+8\kappa_s)\tau_3]\cdot\frac{1}{w^2} \\
& + [(-9-12\kappa_v)+(-9-4\kappa_s)\tau_3]\cdot\frac{1}{w}\tan^{-1}[\frac{w}{2}] \\
& + [(-84-16\kappa_v)+(12-16\kappa_s)\tau_3]\cdot\frac{1}{w^3}\tan^{-1}[\frac{w}{2}] \\
& + [4-(12+16\kappa_s)\tau_3]\cdot\frac{1}{4+w^2} + 128\cdot\frac{3+w^2}{4w^2+w^4}\} \quad (31)
\end{aligned}
$$

Using Eqs. (28 - 31), we can now construct the result of d_2^{inel} from Eq. (20). The result at $\mathcal{O}(p^3)$ for d_2^{inel} is

$$d_2^{\mathcal{O}(p^3)}(Q^2) \;=\; \frac{Q^6}{8M_N^2}\frac{g_A^2}{(4\pi F_\pi)^2 m_\pi^2}\left(\frac{-24-2w^2}{3w^3\sqrt{w^2+4}}\,\sinh^{-1}[\frac{w}{2}] \,+\, \frac{2}{w^2}\right)\,, \tag{32}$$

and the $\mathcal{O}(p^4)$ correction to d_2^{inel} is given by :

$$\begin{aligned} d_2^{\mathcal{O}(p^4)}(Q^2) \;=\; & \frac{Q^6}{8M_N^2}\frac{g_A^2}{(4\pi F_\pi)^2 m_\pi^2}\cdot\frac{m_\pi}{M_N}\cdot\frac{\pi}{32} \\ \times\; & \{[(-8+4\kappa_v)+(-4+8\kappa_s)\tau_3] \\ & +\left[(-57-12\kappa_v+16w^2)+(-9+4\kappa_s)\tau_3\right]\cdot\frac{1}{w^2} \\ & +\frac{1}{2}\left[(9+12\kappa_v)+(9+12\kappa_s)\tau_3\right]\cdot\frac{1}{w}\tan^{-1}[\frac{w}{2}] \\ & +\left[(18+24\kappa_v)+(18-8\kappa_s)\tau_3\right]\cdot\frac{1}{w^3}\tan^{-1}[\frac{w}{2}] \\ & +\left[2+64\cdot\frac{3+w^2}{w^2}-(6+8\kappa_s)\tau_3\right]\cdot\frac{1}{4+w^2}\Bigg\}\,. \end{aligned} \tag{33}$$

Analogously, we can also construct the results for $\Gamma_1^{(3)\,inel}$ and $\Gamma_2^{(3)\,inel}$ of Eqs. (23,26) in HBChPT by using the expressions of Eqs. (28 - 31). The result at $\mathcal{O}(p^3)$ are given by :

$$\Gamma_1^{(3)\,\mathcal{O}(p^3)}(Q^2) \;=\; \frac{Q^6}{4M_N^2}\frac{g_A^2}{(4\pi F_\pi)^2 m_\pi^2}\left(\frac{12+4w^2}{3w^3\sqrt{w^2+4}}\,\sinh^{-1}[\frac{w}{2}] \,-\, \frac{1}{w^2}\right)\,, \tag{34}$$

$$\Gamma_2^{(3)\,\mathcal{O}(p^3)}(Q^2) \;=\; -\frac{Q^6}{4M_N^2}\frac{g_A^2}{(4\pi F_\pi)^2 m_\pi^2}\left(\frac{4+w^2}{w^3\sqrt{w^2+4}}\,\sinh^{-1}[\frac{w}{2}] \,-\, \frac{1}{w^2}\right)\,, \tag{35}$$

and the $\mathcal{O}(p^4)$ corrections are given by :

$$\begin{aligned} \Gamma_1^{(3)\,\mathcal{O}(p^4)}(Q^2) \;=\; & \frac{Q^6}{8M_N^2}\frac{g_A^2}{(4\pi F_\pi)^2 m_\pi^2}\cdot\frac{m_\pi}{M_N}\cdot\frac{\pi}{64} \\ \times\; & \{[(-40+4\kappa_v)+(-4+8\kappa_s)\tau_3] \\ & +\left[(33+36\kappa_v)+(9+4\kappa_s)\tau_3\right]\cdot\frac{1}{w^2} \\ & +\frac{1}{2}\left[(-45-60\kappa_v)+(-45-36\kappa_s)\tau_3\right]\cdot\frac{1}{w}\tan^{-1}[\frac{w}{2}] \\ & +\left[(-162-72\kappa_v)+(-18-8\kappa_s)\tau_3\right]\cdot\frac{1}{w^3}\tan^{-1}[\frac{w}{2}] \\ & +\left[2+64\cdot\frac{3+w^2}{w^2}-(6+8\kappa_s)\tau_3\right]\cdot\frac{1}{4+w^2}\Bigg\}\,, \end{aligned} \tag{36}$$

$$\Gamma_2^{(3)\,\mathcal{O}(p^4)}(Q^2) \;=\; \frac{Q^6}{8M_N^2}\frac{g_A^2}{(4\pi F_\pi)^2 m_\pi^2}\cdot\frac{m_\pi}{M_N}\cdot\frac{\pi}{32}$$

$$\times \left\{ \left[(-30 - 16\kappa_v + 16w^2) - 6\tau_3 \right] \cdot \frac{1}{w^2} \right.$$
$$+ [(9 + 12\kappa_v) + (9 + 8\kappa_s)\tau_3] \cdot \frac{1}{w} \tan^{-1}[\frac{w}{2}]$$
$$\left. + [(60 + 32\kappa_v) + 12\tau_3] \cdot \frac{1}{w^3} \tan^{-1}[\frac{w}{2}] \right\} . \qquad (37)$$

From Eqs. (32 - 37), one can extract that the following prediction of HBChPT in the limit $Q^2 \to 0$:

$$\begin{aligned} d_2^{inel}(Q^2) &\longrightarrow \frac{Q^6}{8M_N^2} \frac{1}{2\alpha_{em}} \left(-\gamma_0(0) + 3\delta_{LT}(0)\right) \\ &= \frac{Q^6}{48M_N^2} \frac{g_A^2}{(4\pi F_\pi)^2 \, m_\pi^2} \left\{ 1 + \frac{m_\pi}{M_N} \cdot \frac{\pi}{8} \left[(21 + 9\kappa_v) + (-6 + 14\kappa_s)\tau_3 \right] \right\} . \quad (38) \\ \Gamma_1^{(3)\,inel}(Q^2) &\longrightarrow \frac{Q^6}{8M_N^2} \frac{1}{2\,\alpha_{em}} \gamma_0(0) \\ &= \frac{Q^6}{48M_N^2} \frac{g_A^2}{(4\pi F_\pi)^2 \, m_\pi^2} \left\{ 2 + \frac{m_\pi}{M_N} \cdot \frac{\pi}{4} \left[(-15 - 3\kappa_v) + (-6 - \kappa_s)\tau_3 \right] \right\} , \quad (39) \\ \Gamma_2^{(3)\,inel}(Q^2) &\longrightarrow \frac{Q^6}{8M_N^2} \frac{1}{2\,\alpha_{em}} \left(-\gamma_0(0) + \delta_{LT}(0)\right) \\ &= \frac{Q^6}{48M_N^2} \frac{g_A^2}{(4\pi F_\pi)^2 \, m_\pi^2} \left\{ -1 + \frac{m_\pi}{M_N} \cdot \frac{\pi}{8} \left[(27 + 7\kappa_v) + (6 + 6\kappa_s)\tau_3 \right] \right\} , \quad (40) \end{aligned}$$

where $\gamma_0(0)$ is the forward spin polarizability at the real photon point, which has also been calculated in HBChPT to $\mathcal{O}(p^4)$, see Ref. [7].

We have also studied the contribution of the $\Delta(1232)$ resonance in the "small scale expansion" $\mathcal{O}(\epsilon^3)$, which uses the quantity $\Delta = M_\Delta - M_N$ as a further expansion parameter. Our results for the quantities I_1, I_A and δ_{LT} are :

$$\begin{aligned} I_1^\Delta(Q^2) &= 0, \\ I_A^\Delta(Q^2) &= \frac{-Q^2}{18} (\frac{G_1}{\Delta})^2 \\ &- \frac{8Q^2M^2}{9} \frac{g_{\pi\Delta N}^2}{(4\pi F_\pi)^2} \int_0^1 dx \frac{x^2(1-2x)}{m_0^2} (\mu_0^2 - 1)^{-1} \left[1 - \mu_0 \frac{\ln[\mu_0 + \sqrt{\mu_0^2 - 1}]}{\sqrt{\mu_0^2 - 1}} \right] \}, \quad (41) \\ \delta_{LT}^\Delta(Q^2) &= \frac{-32\alpha_{em}}{27} \frac{g_{\pi\Delta N}^2}{(4\pi F_\pi)^2} \int_0^1 dx \, \frac{x^3}{m_0^2} (\mu_0^2 - 1)^{-2} \left[\mu_0^2 + 2 - 3\mu_0 \frac{\ln[\mu_0 + \sqrt{\mu_0^2 - 1}]}{\sqrt{\mu_0^2 - 1}} \right] \\ &+ \frac{16\alpha_{em}}{9} \frac{g_{\pi\Delta N}^2}{(4\pi F_\pi)^2} \int_0^1 dx \, \frac{x^2(1-2x)}{m_0^2} (\mu_0^2 - 1)^{-1} \left[1 - \mu_0 \frac{\ln[\mu_0 + \sqrt{\mu_0^2 - 1}]}{\sqrt{\mu_0^2 - 1}} \right] , \quad (42) \end{aligned}$$

with $m_0 \equiv \sqrt{m_\pi^2 + x(1-x)Q^2}$ and $\mu_0 \equiv \frac{\Delta}{m_0}$. Furthermore, G_1 and $g_{\pi\Delta N}$ are the leading order $\gamma\Delta N$ and $\pi\Delta N$ coupling constants respectively. In the large N_C limit of QCD, they

are related with κ_v and g_A as :

$$G_1 = \frac{3}{2\sqrt{2}}\kappa_v, \quad g_{\pi\Delta N} = \frac{3}{2\sqrt{2}}g_A. \tag{43}$$

Furthermore, the $\mathcal{O}(\epsilon^3)$ Δ contribution to d_2 is

$$\begin{aligned} d_2^{\Delta}(Q^2) \; = \; & \frac{Q^6}{8M_N^2}\left\{\frac{1}{18}(\frac{G_1}{M_N})^2 \cdot \frac{1}{\Delta^2}\right. \\ & -\frac{32}{27}\frac{g^2_{\pi\Delta N}}{(4\pi F_\pi)^2}\int_0^1 dx\; \frac{x^3}{m_0^2}(\mu_0^2-1)^{-2}\left[\mu_0^2+2-3\mu_0\frac{\ln[\mu_0+\sqrt{\mu_0^2-1}]}{\sqrt{\mu_0^2-1}}\right] \\ & \left. +\frac{24}{9}\frac{g^2_{\pi\Delta N}}{(4\pi F_\pi)^2}\int_0^1 dx\; \frac{x^2(1-2x)}{m_0^2}(\mu_0^2-1)^{-1}\left[1-\mu_0\frac{\ln[\mu_0+\sqrt{\mu_0^2-1}]}{\sqrt{\mu_0^2-1}}\right]\right\}, \end{aligned} \tag{44}$$

and the $\mathcal{O}(\epsilon^3)$ Δ contribution to $\Gamma_1^{(3)\,inel}$ is

$$\begin{aligned} \Gamma_1^{(3)\,\Delta}(Q^2) \; = \; & \frac{Q^6}{8M_N^2}\left\{\frac{-1}{18}(\frac{G_1}{M_N})^2 \cdot \frac{1}{\Delta^2}\right. \\ & \left. -\frac{16}{27}\frac{g^2_{\pi\Delta N}}{(4\pi F_\pi)^2}\int_0^1 dx\; \frac{x^3}{m_0^2}(\mu_0^2-1)^{-2}\left[\mu_0^2+2-3\mu_0\frac{\ln[\mu_0+\sqrt{\mu_0^2-1}]}{\sqrt{\mu_0^2-1}}\right]\right\}. \end{aligned} \tag{45}$$

In the limit $Q^2 \to 0$, these quantities approache the values

$$\begin{aligned} d_2^{\Delta}(Q^2) \; \longrightarrow \; & \frac{Q^6}{8M_N^2}\left\{\frac{1}{16}(\frac{\kappa_v}{M_N})^2 \cdot \frac{1}{\Delta^2}\right. \\ & -\frac{1}{3}\frac{g_A^2}{(4\pi F_\pi)^2 m_\pi^2}(\mu^2-1)^{-2}\left[\mu^2+2-3\mu\frac{\ln[\mu+\sqrt{\mu^2-1}]}{\sqrt{\mu^2-1}}\right] \\ & \left. -\frac{1}{2}\frac{g_A^2}{(4\pi F_\pi)^2 m_\pi^2}(\mu^2-1)^{-1}\left[1-\mu\frac{\ln[\mu+\sqrt{\mu^2-1}]}{\sqrt{\mu^2-1}}\right]\right\}, \end{aligned} \tag{46}$$

$$\begin{aligned} \Gamma_1^{(3)\,\Delta}(Q^2) \; \longrightarrow \; & \frac{Q^6}{8M_N^2}\left\{\frac{-1}{16}(\frac{\kappa_v}{M_N})^2 \cdot \frac{1}{\Delta^2}\right. \\ & \left. -\frac{1}{6}\frac{g_A^2}{(4\pi F_\pi)^2 m_\pi^2}(\mu^2-1)^{-2}\left[\mu^2+2-3\mu\frac{\ln[\mu+\sqrt{\mu^2-1}]}{\sqrt{\mu^2-1}}\right]\right\}, \end{aligned} \tag{47}$$

with $\mu = \frac{\Delta}{m_\pi}$. Analogous formulae can be derived for $\Gamma_2^{(3)\,\Delta}(Q^2)$ by taking the combination of Eq. (27).

IV. MULTIPOLE CONTENT OF THE MOMENTS

By use of Eqs. (13,14), we can express the moment d_2 by the partial cross sections σ_{TT} and σ_{LT} :

$$d_2^{inel}(Q^2) = \frac{Q^6}{32\pi^2\alpha_{em}M_N^2}\int_{\nu_0}^{\infty} d\nu\, \frac{K(\nu,Q^2)}{\nu^2(\nu^2+Q^2)}\left(-\sigma_{TT}(\nu,Q^2) + \frac{3\nu^2+2Q^2}{\nu Q}\,\sigma_{LT}(\nu,Q^2)\right)\ , \tag{48}$$

and the multipole content follows by inserting the expansion of these cross sections in terms of the electric (E), magnetic (M), and Coulomb or scalar (S) multipoles [24]

$$\begin{aligned} K\sigma_{TT}(1\pi) &= x_{TT}\sum_l \frac{1}{2}(l+1)\Big[(l+2)(|E_{l+}|^2+|M_{l+1,-}|^2) \\ &\quad -l(|E_{l+1,-}|^2+|M_{l+}|^2)+2l(l+2)(E_{l+}^*M_{l+}-E_{l+1,-}^*M_{l+1,-})\Big] \\ &= x_{TT}\left(|E_{0+}|^2+|M_{1-}|^2-|M_{1+}|^2+6E_{1+}^*M_{1+}+3|E_{1+}|^2\pm\ ...\right)\ , \end{aligned} \tag{49}$$

$$\begin{aligned} K\sigma_{LT}(1\pi) &= x_{LT}\sum_l \frac{1}{2}(l+1)^2 \\ &\quad \cdot\Big[S_{l+}^*((l+2)E_{l+}+lM_{l+})+S_{l+1,-}^*(lE_{l+1,-}-(l+2)M_{l+1,-})\Big] \\ &= x_{LT}\left(S_{0+}^*E_{0+}-S_{1-}^*M_{1-}+2S_{1+}^*(M_{1+}+3E_{1+})\pm\ ...\right)\ , \end{aligned} \tag{50}$$

where

$$x_{TT} = x_{TT}(\nu,Q^2) = 4\pi\sqrt{(\nu-\nu_0)\,(\nu-\nu_0+2m_\pi)}\ , \tag{51}$$

$$x_{LT} = x_{LT}(\nu,Q^2) = \sqrt{\frac{1+2\nu/M_N-Q^2/M_N^2}{1+\nu^2/Q^2}}\,x_{TT}(\nu,Q^2)\ . \tag{52}$$

The multipoles are generally functions of the *cm* energy of the photon, $\mathcal{M}_{l\pm}(\omega,Q^2)$, with

$$\omega = \frac{M_N\nu-Q^2}{\sqrt{2M_N\nu+M_N^2-Q^2}}\ . \tag{53}$$

In comparing with Ref. [24] it should be noted that we have changed the sign of the partial cross sections in order to stay in accordance with the usual notation of deep inelastic scattering, i.e., $\sigma_{TT}=-\sigma'_{TT}$ and $\sigma_{LT}=-\sigma'_{LT}$, where σ'_{TT} and σ'_{LT} were used in Ref. [24]. We also note that expressions like $S_{0+}^*E_{0+}$ should be read as $\mathrm{Re}\,(S_{0+}^*E_{0+})$.

The expression for the moments $\Gamma_1^{(3)}$, $\Gamma_2^{(3)}$ and f_2 can be derived similarly as Eq. (48).

$$\Gamma_1^{(3)\,inel}(Q^2) = \frac{Q^6}{32\pi^2\alpha_{em}M_N^2}\int_{\nu_0}^{\infty} d\nu\,\frac{K(\nu,Q^2)}{\nu^2(\nu^2+Q^2)}\left(\sigma_{TT}(\nu,Q^2)+\frac{Q}{\nu}\sigma_{LT}(\nu,Q^2)\right)\ , \tag{54}$$

$$\Gamma_2^{(3)\,inel}(Q^2) \;=\; \frac{Q^6}{32\pi^2\alpha_{em}M_N^2}\int_{\nu_0}^{\infty} d\nu\,\frac{K(\nu,Q^2)}{\nu^2(\nu^2+Q^2)}\left(-\sigma_{TT}(\nu,Q^2)+\frac{\nu}{Q}\sigma_{LT}(\nu,Q^2)\right)\,, \tag{55}$$

$$\begin{aligned} f_2^{inel}(Q^2) \;=\; & -\frac{9Q^2}{4M_N^2}\,\Gamma^{(1)}_{1,\,tw-2} + \frac{9Q^4}{32\pi^2\alpha_{em}M_N^2}\int_{\nu_0}^{\infty} d\nu\,\frac{K(\nu,Q^2)}{\nu^2+Q^2}\left(\sigma_{TT}(\nu,Q^2)+\frac{Q}{\nu}\sigma_{LT}(\nu,Q^2)\right) \\ & + \frac{Q^6}{64\pi^2\alpha_{em}M_N^2}\int_{\nu_0}^{\infty} d\nu\,\frac{K(\nu,Q^2)}{\nu^2(\nu^2+Q^2)}\left(\sigma_{TT}(\nu,Q^2)-\frac{3(\nu^2+Q^2)}{Q\nu}\sigma_{LT}(\nu,Q^2)\right)\,. \end{aligned} \tag{56}$$

V. RESULTS AND DISCUSSION

In Fig. 1, we show the results for the Q^2 dependence of the moment d_2. At large Q^2, the values of d_2 have been obtained for both proton and neutron by DIS experiments at SLAC using a transversely polarized target [3]. From these experiments, the following values have been extracted at an average value of $Q^2 = 5$ GeV^2 [3] :

$$\begin{aligned} d_2^p(Q^2 \approx 5\,\mathrm{GeV}^2) &= 0.0032 \pm 0.0017\,, \\ d_2^n(Q^2 \approx 5\,\mathrm{GeV}^2) &= 0.0079 \pm 0.0048\,. \end{aligned} \tag{57}$$

In the low and intermediate Q^2 region, we show the results for d_2 according to the generalized definition of Eq. (9). It rises strongly at the lower Q^2, displaying a Q^6 dependence at low Q^2, and tending to a small constant value asymptotically, corresponding with the twist-3 matrix element entering in the OPE of Eq. (3). Due to this structure, d_2 is an interesting observable to interpolate between a hadronic description at low Q^2 and a partonic description at large Q^2 values. One sees from Fig. 1 that the ChPT results rise strongly with Q^2, and its Q^6 dependence at the low Q^2 values is given by Eq. (38). The large difference between the $O(p^3)$ and $O(p^4)$ results originates from the known large difference between the $O(p^3)$ and $O(p^4)$ HBChPT results for the forward spin polarizability γ_0 [28, 29, 30]. It is interesting to note however that the $O(p^3)$ HBChPT result is in good agreement with the phenomenological MAID estimate up to $Q^2 \simeq 0.25$ GeV^2. The convergence of the heavy baryon chiral expansion for the forward spin polarizability has been recently investigated in Ref. [9] using the Lorentz invariant formulation of baryon ChPT of Ref. [31]. It was found [9] that the main reason for the slow convergence of γ_0 in the $1/M_N$ expansion is due to the slow convergence of the Born graphs. The corresponding one-loop relativistic calculation cures this deficiency. However the relativistic result to fourth order in the chiral expansion, even when supplemented with Δ and vector meson contributions, still does not agree with

the data, suggesting to envisage a fifth-order calculation for γ_0 in future work.

Very recently, the inelastic contribution to d_2 has been measured for the neutron at intermediate Q^2 values at JLab/Hall A [4]. It is seen from Fig. 1 that the phenomenological resonance prediction using the MAID model for the neutron shows an excellent agreement with these data. We will discuss the MAID results for d_2^n further on, to get some better understanding of the origin of this good description.

In Figs. 2 and 3, we show the results for the Q^2 dependence of the third moments of the nucleon spin structure functions g_1 and g_2 respectively. From Eqs. (39,40), we see that the inelastic part to the moment $\Gamma_1^{(3)}$ is proportional to $Q^6 \cdot \gamma_0$ at small Q^2, and that the inelastic part to the moment $\Gamma_2^{(3)}$ also contains γ_0 at small Q^2. Therefore the HBChPT results for those moments directly reflect the poor convergence of the chiral expansion for γ_0. The MAID model predicts a value for γ_0 at the real photon point as : $\gamma_0^p = -0.707 \cdot 10^{-4}\mathrm{fm}^4$, which is in relative good agreement with the experimental value (for its determination, see Ref. [6]) :

$$\gamma_0^p = [-1.01 \pm 0.08 \text{ (stat)} \pm 0.10 \text{ (syst)}] \cdot 10^{-4} \text{ fm}^4 \;. \tag{58}$$

Going to larger values of Q^2, the MAID results for the proton change sign. At large Q^2, the value of $\Gamma_1^{(3)}$ is known from DIS experiments as shown on Fig. 2. We also compare in Fig. 2 the MAID result with the resonance contribution to $\Gamma_1^{(3)}$ (corresponding with $W < 2$ GeV) as extracted from the fit of g_1 data. From this comparison, we see that the π-channel alone underestimates the total resonance contribution at larger Q^2. For the proton channel, we are also able to provide an estimate for the ηN and $\pi\pi N$ channels which provide the dominant virtual photon absorption cross sections beyond πN. It is seen that the sum of the $\pi + \pi\pi + \eta$ channels nicely joins the $W < 2$ GeV part of the DIS parametrization (lower shaded band in Fig. 2) for $Q^2 > 3$ GeV^2. To gain an understanding of the gradual transition in $\Gamma_1^{(3)}$, from the resonance dominated to the partonic regime, we generalize a suggestion of Ref. [33] for the first moment I_1 of g_1 to parametrize its Q^2 dependence through a vector meson dominance type model. This model for I_1 was refined in Refs. [34, 35] by adding explicit resonance contributions which are important at low Q^2 as seen above. We can generalize this phenomenological parametrization for the inelastic part to an arbitrary moment of g_1 through the interpolating formula :

$$\Gamma_1^{(n)\,inel}(Q^2) \;=\; \Gamma_1^{(n)\,res}(Q^2) + \frac{(Q^2)^n}{(Q^2+\mu^2)^{n+1}} \left(Q^2\,\Gamma_1^{(n)\,as} \,+\, \mu^2\, c^{(n)} \right) , \tag{59}$$

where $\Gamma_1^{(n)\,res}(Q^2)$ is the resonance contribution evaluated using the MAID model, and μ is a vector meson mass scale ($\mu \approx 0.77$ GeV), which governs the transition to the asymptotic value $\Gamma_1^{(n)\,as}$. The coefficient $c^{(n)}$ is chosen in such a way that $\Gamma_1^{(n)}$ reaches its known value at the real photon point. For $c^{(1)}$, this is fixed by the non-resonant contribution to the GDH sum rule as :

$$c^{(1)} \;=\; \frac{\mu^2}{2\,M_N^2}\,\left(-\kappa^2/4 \;-\; I_1^{res}(0)\right), \tag{60}$$

where $I_1^{res}(0)$ is the resonance contribution ($W < 2$ GeV) at the real photon point to I_1. For the third moment, the coefficient $c^{(3)}$ is fixed by the very small non-resonant contribution to the forward spin polarizability :

$$c^{(3)} \;=\; \frac{(\mu^2)^3}{16\,M_N^2}\,\frac{1}{\alpha_{em}}\,\left(\,\gamma_0(0) \;-\; \gamma_0^{res}(0)\,\right), \tag{61}$$

where $\gamma_0^{res}(0)$ is the resonance contribution (corresponding with $W < 2$ GeV). Analogously, one can express the coefficients $c^{(n)}$ for higher moments ($n = 5, 7, ...$) through the very small non-resonant contributions to the higher spin polarizabilities of the nucleon. As these higher polarizabilities are practically completely dominated by the low-energy excitation region (i.e. resonance region), it is a very good approximation to take $c_1^{(n)} \simeq 0$ for $n \geq 5$.

In Fig. 2, we also show the result of the interpolating model of Eq. (59) for $\Gamma_1^{(3)}$ of the proton, by using the MAID model for the resonance contribution $\Gamma_1^{(3)\,res}$ and using as asymptotic contribution for the proton : $\Gamma_1^{(3)\,as} \simeq 0.012$. It will be interesting to compare these predictions with experimental results which can be extracted from corresponding analyses for the lowest moments of the proton [36] and neutron [37] structure function g_1.

Besides the inelastic contributions, we also show in Figs. 1,2 for comparison the elastic contributions to d_2 and $\Gamma_1^{(3)}$ according to Eqs. (11,21). The elastic contribution is calculated by using for the proton the form factor parametrization of Ref. [38] including the new JLab data for the ratio of G_E^p/G_M^p [39, 40]. For the neutron, the elastic contribution is calculated using for G_E^n the recent fit of Ref. [41] (following the Galster form), and for G_M^n the recent fit of Ref. [42]. We see from Fig. 1 that for the proton the elastic contribution largely dominates the inelastic one for both d_2 and $\Gamma_1^{(3)}$ when $Q^2 < 1$ GeV^2. For the neutron, the elastic contributions to d_2 and $\Gamma_1^{(3)}$ are of comparable size to the inelastic ones and vanish at the real photon point.

In Fig. 4, we show the separate contributions of σ_{TT} and σ_{LT} to d_2^n and $\Gamma_1^{(3)n}$ to gain

some insight in the nature of the photon absorption mechanism involved. In the case of the twist-3 moment d_2 of Eq. (48), σ_{LT} is enhanced by the kinematical term in front, and therefore becomes dominant at large values of ν and Q^2. The situation is quite different for the third moment $\Gamma_1^{(3)n}$ of Eq. (54), in which case the LT term vanishes at $Q^2 = 0$ and is suppressed for large ν.

The multipole content of d_2 is displayed in Fig. 5 for both proton and neutron. This moment is dominated by an interplay of s- and p-wave multipoles up to $Q^2 \approx 4$ GeV^2. The striking difference between the proton and neutron is essentially due to the excitation of the $S_{11}(1535)$ resonance. According to the Particle Data Group [18], the helicity amplitudes for the $S_{11}(1535)$ are $A^p_{1/2} = (0.090 \pm 0.030)$ GeV$^{-1/2}$ and $A^n_{1/2} = (-0.046 \pm 0.027)$ GeV$^{-1/2}$, with the result that the cross sections for S_{11} excitation on the proton are about a factor 4 larger as compared to the neutron. It is also known that this resonance has a very hard form factor [43, 44], and therefore this effect persists up to very high momentum transfers. This leads to the difference that d_2^p changes sign around $Q^2 \approx 1.25$ GeV^2, whereas d_2^n remains at the same sign as confirmed by the data.

Fig. 6 shows the multipole analysis for the moment $\Gamma_1^{(3)n}$. The conclusions are similar as in the previous case. The strong coupling of the S_{11} to the proton leads to the distinct feature that $\Gamma_1^{(3)p}$ changes sign at $Q^2 \approx 1.25$ GeV^2 and asymptotically remains at larger values than for the neutron.

In Fig. 7, we show our result for f_2 as extracted from Eq. (10). To calculate f_2, we need the full Q^2 dependence of $\Gamma_1^{(1)}$ consisting of a sum of elastic and inelastic contributions. The elastic contribution is given by Eq. (21) and evaluated using the most recent experimental information on the nucleon form factors as detailed above. The inelastic contribution can e.g. be obtained by using the interpolating formula of Eq. (59). Although this gives a decent description of both proton and neutron data, a better fit for the proton data is obtained by using as interpolating formula :

$$\Gamma_1^{(1)\,inel}(Q^2) \;=\; \Gamma_1^{(1)\,res}(Q^2) \,+\, \Gamma_1^{(1)\,as}\,\tanh\left(\frac{Q^2\,(Q^2+\mu^2\,c^{(1)}/\Gamma_1^{(1)\,as})}{\mu^2\,(Q^2+\mu^2)}\right)\,, \tag{62}$$

where $c^{(1)}$ is as defined in Eq. (60), with $I_1^{res,p}(0) = -0.67$ obtained from the MAID model. Furthermore, we fix the asymptotic value by using $\Gamma_1^{(1)\,p} = 0.118$ at $Q^2 = 5$ GeV^2, as obtained from the global analysis of Ref. [45]. This value then fixes the asymptotic coefficient $\Gamma_1^{(1)\,as}$ in the interpolating formula for $\Gamma_1^{(1)\,inel}$, as well as the flavor singlet axial charge a_0^∞ in the

twist-2 part $\Gamma^{(1)}_{1,\,tw-2}$ of Eq. (4). The shape parameter μ in Eq. (62) is taken as $\mu \simeq 0.74$ GeV, which gives a very good description of all proton data for $\Gamma_1^{(1)\,inel}$ as seen from Fig. 7. Note that we merely consider the functional form of Eq. (62) as a convenient representation of the inelastic data.

For the neutron, we use the interpolating formula of Eq. (59), with $I_1^{res,\,n}(0) = -0.48$ obtained from the MAID model. Furthermore, we use as asymptotic value $\Gamma_1^{(1)\,as,n} = -0.038$, and mass scale $\mu \simeq 0.57$ GeV. Note that in order to get a good description of the JLab/Hall A data of Ref. [37], we use an asymptotic value which is somewhat smaller in absolute value than the value $\Gamma_1^{(1)\,n}(Q^2 = 5\ \mathrm{GeV}^2) = -0.058 \pm 0.005 \pm 0.008$ as obtained from the global analysis of Ref. [45].

Furthermore in Fig. 7, we also show separately the twist-2 part $\Gamma^{(1)}_{1,\,tw-2}$, and the term $(a_2 + 4d_2) \cdot M_N^2/(9Q^2)$, which is seen to be negligibly small for both proton and neutron. Therefore f_2 is dominated by the difference $\Gamma_1^{(1)\,el} + \Gamma_1^{(1)\,inel} - \Gamma^{(1)}_{1,\,tw-2}$. The quantity $f_2 \cdot 4M_N^2/(9Q^2)$ evaluated using Eq. (10) is shown by the thick solid curves in Fig. 7. We can then extract f_2 from the linear regime in the $1/Q^2$ plot. Because the slight non-linear structure observed in the thick solid curves in Fig. 7 is within the error bars of the data, we make a linear fit by including all data for Q^2 in the range $0.5 - 2$ GeV^2, in particular the new JLab data for both proton and neutron. This is shown by the shaded bands in the same figure, which fully accomodate the thick solid curves in the mentioned Q^2 range. From the slopes of these bands, we can then extract f_2 for Q^2 in the range 0.5 - 2 GeV^2 as :

$$\begin{aligned} f_2^p &\simeq 0.15 \to 0.18\,, \\ f_2^n &\simeq -0.026 \to -0.013\,. \end{aligned} \tag{63}$$

The twist-4 matrix elements f_2 have been extracted before in Ref. [11] from the data of Ref. [2] at $Q^2 = 1$ GeV^2, resulting in the values [51] :

$$\begin{aligned} f_2^p &= 0.10 \pm 0.05\ , \\ f_2^n &= 0.07 \pm 0.08\ . \end{aligned} \tag{64}$$

Comparing our results of Eq. (63) with those of Ref. [11], we see that they are compatible for the proton but that we extract a small negative value for the neutron, whereas in Ref. [11] a positive result was extracted. However, given the uncertainty of the neutron data both values of f_2^n might well be consistent with zero. One sees from Fig. 7, that for the neutron

there is a partial cancellation between the elastic and inelastic contribution to $\Gamma_1^{(1)}$, and the result for f_2 is practically completely given by the resonance contribution $\Gamma_1^{(1)\,res}$, which is estimated here in the MAID model and gives a good description of the available neutron data as we have seen before. This might partly explain why we extract a negative value for f_2^n, compared with the analysis of Ref. [11].

We can compare these phenomenological values for f_2 with several model estimates. In Ref. [23], an estimate was given within QCD sum rules which yielded as values : $f_2^p = -0.037 \pm 0.006$ and $f_2^n = -0.013 \pm 0.006$. In Ref. [21], the instanton vacuum picture was used to estimate matrix elements of quark gluon operators. In particular it has been shown in this approach that the matrix element d_2 is suppressed relative to f_2 as :

$$\frac{d_2}{f_2} \sim \left(\frac{\bar{\rho}}{\bar{R}}\right)^4 << 1\,, \tag{65}$$

where $\bar{\rho}/\bar{R} \simeq 1/3$ is the average instanton density. Using the $SU(3)$ symmetric case, the twist-4 matrix elements f_2 were obtained in Ref. [21] as : $f_2^p = -0.046$ and $f_2^n = +0.038$. We notice that in the approach of Ref. [21], proton and neutron values are of comparable size and opposite sign. In both the QCD sum rules and instanton vacuum models, the proton value is smaller and of opposite sign compared with the phenomenologically extracted value of Ref. [11] and with the value Eq. (63) of this work.

It has been suggested that the twist-3 moment d_2 and the twist-four moment f_2 are related to the response of the color electric (χ_E) and magnetic (χ_B) fields to the polarization of the nucleon in its rest frame [48, 49], defined as :

$$\begin{aligned} \langle PS|\psi^\dagger\, g\vec{B}\,\psi|PS\rangle &= \chi_B\, 2M_N^2\, \vec{S}\,, \\ \langle PS|\psi^\dagger\, \vec{\alpha}\times g\vec{E}\,\psi|PS\rangle &= \chi_E\, 2M_N^2\, \vec{S}\,, \end{aligned} \tag{66}$$

where P is the nucleon momentum and S the projection of its spin vector $\vec{S}$. Furthermore $\vec{E}$ ($\vec{B}$) are the color electric (magnetic) fields respectively, and g is the strong coupling constant. Furthermore, the moments d_2 and f_2 can be expressed in terms of the gluon-field polarizabilities as :

$$\begin{aligned} d_2 &= \frac{1}{4}\left(\chi_E + 2\chi_B\right)\,, \\ f_2 &= \left(\chi_E - \chi_B\right)\,. \end{aligned} \tag{67}$$

Since the experimental value of d_2 is of order 10^{-3}, we see from Eq. (63) that the predicted central values of f_2 are larger than those of d_2 by about a factor 50 for the proton. These

findings agree, at least qualitatively, with estimates using QCD sum rules [23] and based on the instanton vacuum approach [21], but less so with the predictions of bag models [14]. Within the large uncertainties of all existing predictions, we may therefore conclude that $d_2 \ll f_2$. This observation can be combined with Eq. (67) to yield

$$\begin{aligned} \chi_E &\approx +\frac{2}{3} f_2 \, , \\ \chi_B &\approx -\frac{1}{3} f_2 \, . \end{aligned} \tag{68}$$

In particular a positive value of f_2, such as found in both the phenomenological extraction of Eq. (63) and Eq. (64) for the proton, leads to a negative value of χ_B, i.e., color diamagnetism.

VI. CONCLUSIONS

In this work we have studied higher moments of nucleon spin structure functions in view of recent data at intermediate values of Q^2. In particular, we evaluated the generalizations to arbitrary momentum transfer Q^2 of the third moment d_2 of the twist-3 part of the nucleon spin structure function g_2, as well as the third moments $\Gamma_1^{(3)}$ and $\Gamma_2^{(3)}$ of g_1 and g_2 respectively. We have shown that the physical interpretation of d_2, $\Gamma_1^{(3)}$, and $\Gamma_2^{(3)}$ at arbitrary values of Q^2 is given through nucleon generalized (i.e. Q^2 dependent) spin polarizabilities. These higher moments in the Bjorken variable x contain appreciable contributions from the resonance region. We therefore evaluated these moments in heavy baryon chiral perturbation theory (HBChPT) at order $\mathcal{O}(p^4)$ and in a unitary isobar model (MAID).

The ChPT results were found to rise strongly with Q^2, and display a Q^6 dependence at low Q^2 values, proportional to the forward spin polarizabilities at the real photon point. For d_2, the $O(p^3)$ HBChPT results are in good agreement with the phenomenological MAID estimate up to $Q^2 \simeq 0.25$ GeV^2. However there is a large difference between the $O(p^3)$ and $O(p^4)$ results. This difference originates from the known large difference between the $O(p^3)$ and $O(p^4)$ HBChPT results for the forward spin polarizability γ_0, for which the chiral expansion is poorly converging.

The phenomenological unitary isobar prediction using the MAID model shows an excellent agreement with recent neutron data from JLab/Hall A at intermediate Q^2 values. The good description is found in part to be due to a sizeable contribution from the σ_{LT} photoabsorption cross section. Furthermore, we performed a multipole expansion of these

higher moments to gain some additional insight in the dominant absorption mechanisms. We found that both d_2 and $\Gamma_1^{(3)}$ are dominated by an interplay of s- and p-wave multipoles up to $Q^2 \approx 4$ GeV^2, and observed a striking difference between the proton and neutron, which is essentially due to the excitation of the $S_{11}(1535)$ resonance. The helicity amplitudes for the photoexcitation of the S_{11} on the proton are about a factor 4 larger as compared to the neutron, and this resonance has a very hard form factor. This leads to the result that both d_2^p and $\Gamma_1^{(3)\,p}$ change sign around $Q^2 \approx 1.25$ GeV^2, and asymptotically remain at much larger values than in the case of the neutron. It will be interesting to test this prediction by extracting d_2 and $\Gamma_1^{(3)}$ from proton data, and to see if one obtains a similar good description as for the neutron.

Besides the twist-3 matrix element d_2, the $1/Q^2$ suppressed term in the twist expansion of the first moment $\Gamma_1^{(1)}$ of g_1 also contains the twist-4 matrix element f_2. By including all data for $\Gamma_1^{(1)}$ for Q^2 in the range $0.5 - 2$ GeV^2, in particular the new JLab data for both proton and neutron, we extracted f_2 in this Q^2 range as : $f_2^p\ :\ 0.15 \rightarrow 0.18$, and $f_2^n\ :\ -0.026 \rightarrow -0.013$.

The values of d_2 and f_2 enter in the response of the color electric and magnetic fields to the polarization of the nucleon in its rest frame. Therefore our numerical estimates yield phenomenological predictions for gluon field polarizabilities, which are new nucleon structure information.

In summary, the sum rules which we studied in this work as function of Q^2 from the real photon point to the region of deep inelastic scattering, are very interesting observables to interpolate between the non-perturbative and perturbative regimes of QCD. As these higher moments do not require large extrapolations into unmeasured regions, they are ideal observables to be measured at intermediate momentum transfers.

Acknowledgements

This work was supported by the Deutsche Forschungsgemeinschaft (SFB443) and by the U.S. Department of Energy under contract DE-AC05-84ER40150. The authors like to thank

G. Cates, J.-P. Chen, S. Choi, Z.-E. Meziani for useful discussions and correspondence.

---

[1] B.W. Filippone and X. Ji, Adv. Nucl. Phys. **26**, 1 (2001).

[2] K. Abe et al., (E143 Collaboration), Phys. Rev. Lett. **76**, 587 (1996).

[3] P.L. Anthony *et al.* (E155 Collaboration), Phys. Lett. B **553**, 18 (2003).

[4] M. Amarian *et al.* (JLab E94010 Collaboration), hep-ex/0310003.

[5] Z.-E. Meziani, S. Choi and X. Jiang, JLab/Hall A proposal PR03-107.

[6] D. Drechsel, B. Pasquini and M. Vanderhaeghen, Phys. Rep. **378**, 99 (2003).

[7] C.W. Kao, Th. Spitzenberg, and M. Vanderhaeghen, Phys. Rev. D **67**, 016001 (2003).

[8] V. Bernard, T.R. Hemmert, and U.-G. Meißner, Phys. Lett. B **545**, 105 (2002).

[9] V. Bernard, T.R. Hemmert, and U.-G. Meißner, Phys. Rev. D **67**, 076008 (2003).

[10] D. Drechsel, O. Hanstein, S. Kamalov, and L. Tiator, Nucl. Phys. **A645**, 145 (1999).

[11] X. Ji and W. Melnitchouk, Phys. Rev. D **56**, R1 (1997).

[12] J. Edelmann, G. Piller, N. Kaiser, W. Weise, Nucl. Phys. **A665**, 125 (2000).

[13] X. Ji, Nucl. Phys. **B402**, 217 (1993).

[14] X. Ji and P. Unrau, Phys. Lett. B **333**, 228 (1994).

[15] S.A. Larin, J. Vermaseren, Phys. Lett. B **259**, 345 (1991).

[16] S.A. Larin, Phys. Lett. B **334**, 192 (1994).

[17] S.A. Larin, T. van Ritbergen, J. Vermaseren, Phys. Lett. B **404**, 153 (1997).

[18] K. Hagiwara *et al.* (Particle Data Group), Phys. Rev. D **66**, 010001 (2002).

[19] Y. Goto *et al.* (Asymmetry Analysis Collaboration), Phys. Rev. D **62**, 034017 (2000).

[20] S. Wandzura and F. Wilczek, Phys. Lett. B **72**, 195 (1977).

[21] N.-Y. Lee, K. Goeke, and C. Weiss, Phys. Rev. D **65**, 054008 (2002).

[22] M. Göckeler *et al.*, Phys. Rev. D **63**, 074506 (2001).

[23] E. Stein, P. Gornicki, L. Mankiewicz, and A. Schäfer, Phys. Lett. B **353**, 107 (1995).

[24] D. Drechsel, S. Kamalov, and L. Tiator, Phys. Rev. D **63**, 114010 (2001).

[25] B.R. Holstein, D. Drechsel, B. Pasquini, and M. Vanderhaeghen, Phys. Rev. C **61**, 034316 (2000).

[26] X. Ji and J. Osborne, J. Phys. G **27**, 127 (2001).

[27] X. Ji, C.-W. Kao, and J. Osborne, Phys. Lett. B **472**, 1 (2000).

[28] X. Ji, C.-W. Kao, and J. Osborne, Phys. Rev. D **61**, 074003 (2000).

[29] K.B. Vijaya Kumar, J.A. McGovern, and M.C. Birse, Phys. Lett. B **479**, 167 (2000).

[30] G.C. Gellas, T.R. Hemmert, and U.-G. Meißner, Phys. Rev. Lett. **85**, 14 (2000).

[31] T. Becher and H. Leutwyler, Eur. Phys. J. C **9**, 643 (1999).

[32] J. Blümlein and H. Böttcher, Nucl. Phys. **B636**, 225 (2002).

[33] M. Anselmino, B.L. Ioffe, and E. Leader, Sov. J. Nucl. Phys. **49**, 136 (1989).

[34] V. Burkert and B.L. Ioffe, Phys. Lett. B **296**, 223 (1992); J. Exp. Theor. Phys. **78**, 619 (1994).

[35] V. Burkert and Zh. Li, Phys. Rev. D **47**, 46 (1993).

[36] R. Fatemi *et al.* (CLAS Collaboration), Phys. Rev. Lett. **91**, 222002 (2003).

[37] M. Amarian *et al.* (JLab E94010 Collaboration), Phys. Rev. Lett. **89**, 242301 (2002).

[38] E.J. Brash, A. Kozlov, Sh. Li, and G.M. Huber, Phys. Rev. C **65**, 051001 (R) (2002).

[39] M.K. Jones *et al.*, Phys. Rev. Lett. **84**, 1398 (2000).

[40] O. Gayou *et al.*, Phys. Rev. Lett. **88**, 092301 (2002).

[41] G. Warren *et al.* (JLab E93-026 Collaboration), nucl-ex/0308021.

[42] G. Kubon *et al.*, Phys. Lett. B **524**, 26 (2002).

[43] C.S. Armstrong *et al.*, Phys. Rev. D **60**, 052004 (1999).

[44] R. Thompson *et al.*, Phys. Rev. Lett. **86**, 1702 (2001).

[45] P.L. Anthony *et al.* (E155 Collaboration), Phys. Lett. B **493**, 19 (2000).

[46] K. Abe *et al.* (E143 Collaboration), Phys. Rev. D **58**, 112003 (1998).

[47] A. Airapetian *et al.* (HERMES Collaboration), Eur. Phys. J. C **26**, 527 (2003).

[48] X. Ji, published in the Proceedings of the *7th International Conference on the Structure of Baryons*, Eds. B.F. Gibson, P.D. Barnes, J.B. McClelland, and W. Weise (World Scientific, Singapore, 1996); hep-ph/9510362.

[49] L. Mankiewicz, E. Stein and A. Schäfer, in Proceeding of *Prospects on spin physics at HERA*; Eds. J. Blümlein and W.-D. Nowak (Hamburg, Germany, DESY, 1995). hep-ph/9510418.

[50] Note that the partial cross sections σ_{TT} and σ_{LT} depend on the virtual photon flux convention. However, in the dispersion integrals only the products $K \cdot \sigma_{TT}$ and $K \cdot \sigma_{LT}$ enter, which are independent of this convention.

[51] Note that in the present work, we follow the opposite sign convention for f_2 as in Ref. [11].

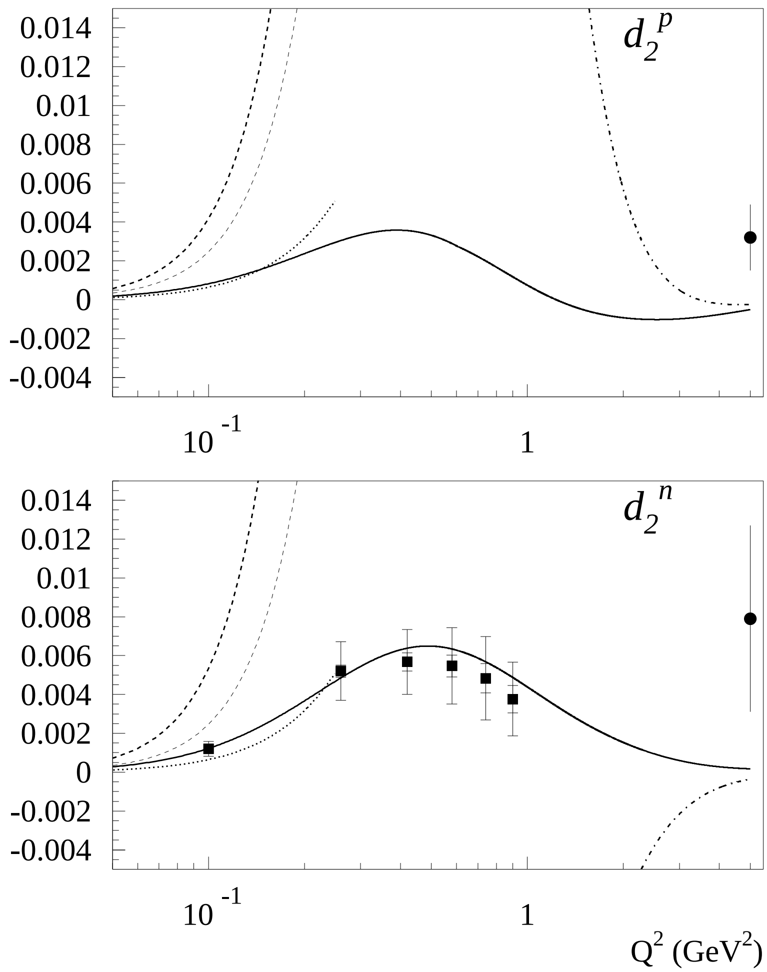

Figure 1: Q^2 dependence of the moment d_2 for proton (upper panel) and neutron (lower panel). The dashed-dotted curve is the elastic contribution to d_2 according to Eq. (11). The other curves represent the inelastic contributions to d_2. Solid curves : MAID estimate for the π channel; dotted curves : $\mathcal{O}(p^3)$ HBChPT; thick (upper) dashed curves : $\mathcal{O}(p^3) + \mathcal{O}(p^4)$ HBChPT; thin (lower) dashed curves : $\mathcal{O}(p^3)$ HBChPT with $\mathcal{O}(\varepsilon^3)$ Δ contribution added. The JLab/Hall A data (diamonds) are from Ref. [4] (inner error bars are statistical errors only, outer error bars include systematical errors). The SLAC data (circles at $Q^2 = 5$ GeV^2) are from Ref. [3].

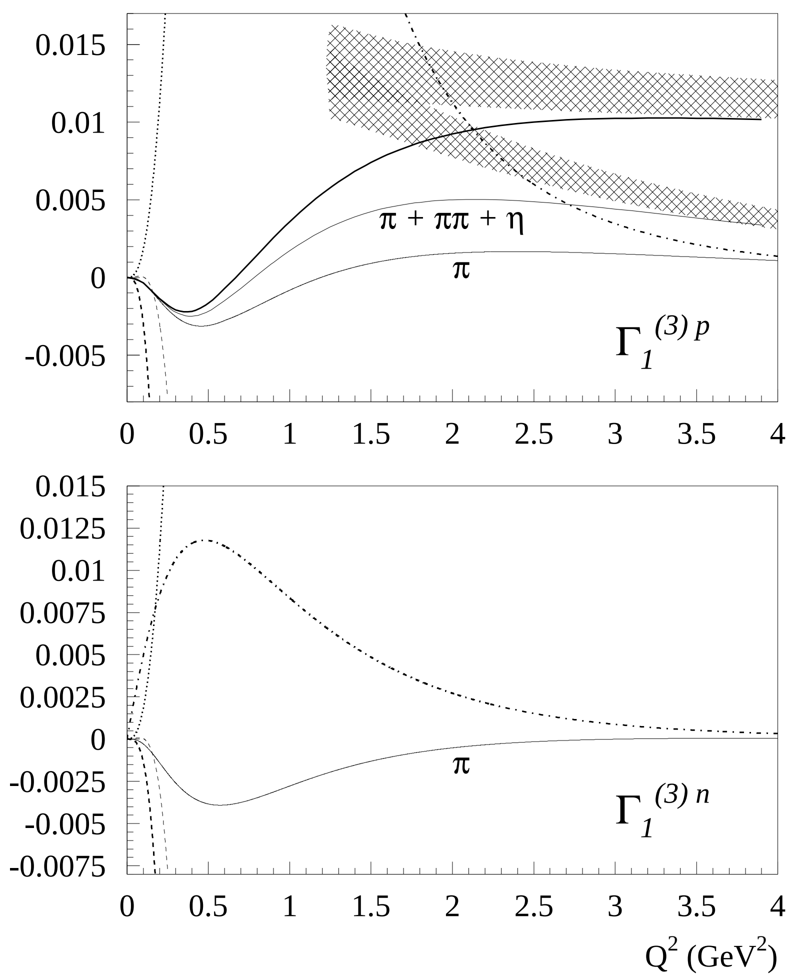

Figure 2: Q^2 dependence of the moment $\Gamma_1^{(3)}$ for proton (upper panel) and neutron (lower panel). The dashed-dotted curve is the elastic contribution to $\Gamma_1^{(3)}$ according to Eq. (21). The other curves represent the inelastic contributions to $\Gamma_1^{(3)}$. Thin solid curves : MAID estimates for the π and $\pi + \pi\pi + \eta$ channels (for proton) as indicated on curves; upper thick solid curve (for proton) : total estimate according to Eq. (59); dotted curves : $\mathcal{O}(p^3)$ HBChPT; thick dashed curves : $\mathcal{O}(p^3) + \mathcal{O}(p^4)$ HBChPT; thin dashed curves : $\mathcal{O}(p^3)$ HBChPT with $\mathcal{O}(\varepsilon^3)$ Δ contribution added. The upper shaded band is the evaluation using the DIS structure function g_1 as extracted from experiment, according to the analyis of Ref. [32]. The lower shaded band is the corresponding analysis for the contribution from the region $W < 2$ GeV (i.e. resonance region) to the DIS parametrization. The size of the bands represents the corresponding (1σ) error estimates as given by Ref. [32].

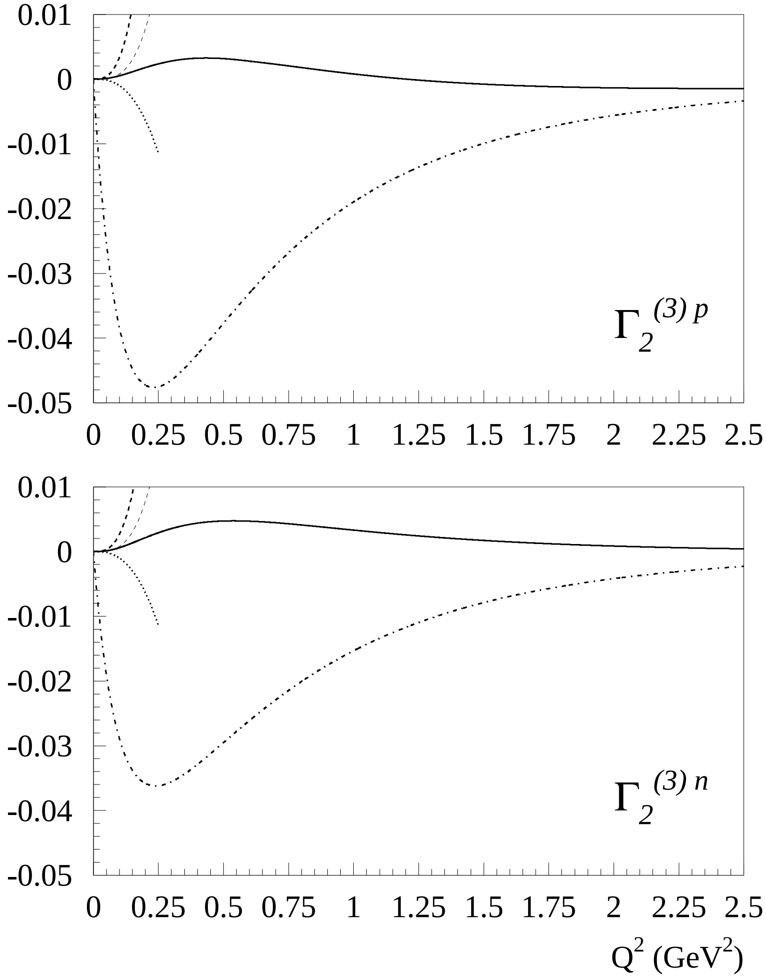

Figure 3: Q^2 dependence of the moment $\Gamma_2^{(3)}$ for proton (upper panel) and neutron (lower panel). The dashed-dotted curves are the elastic contributions to $\Gamma_2^{(3)}$ according to Eq. (24). The other curves represent the inelastic contributions to $\Gamma_2^{(3)}$. Solid curves : MAID estimates for the π channel; dotted curves : $\mathcal{O}(p^3)$ HBChPT; thick dashed curves : $\mathcal{O}(p^3) + \mathcal{O}(p^4)$ HBChPT; thin dashed curves : $\mathcal{O}(p^3)$ HBChPT with $\mathcal{O}(\varepsilon^3)$ Δ contribution added.

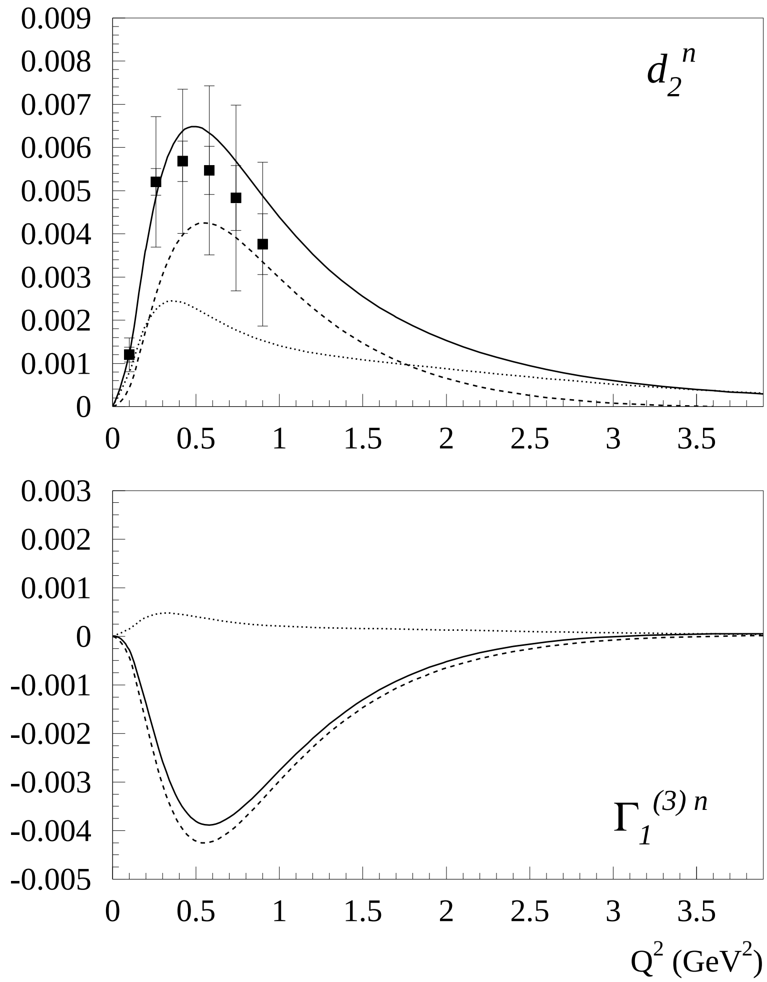

Figure 4: Different photon absorption cross section contributions to d_2 (upper panel) and $\Gamma_1^{(3)}$ (lower panel) for the neutron. The solid curves are the total MAID estimate for the π channel. The dashed (dotted) curves are the contributions from σ_{TT} (σ_{LT}) separately in Eqs. (48) and (54). Data for d_2 as in Fig. 1.

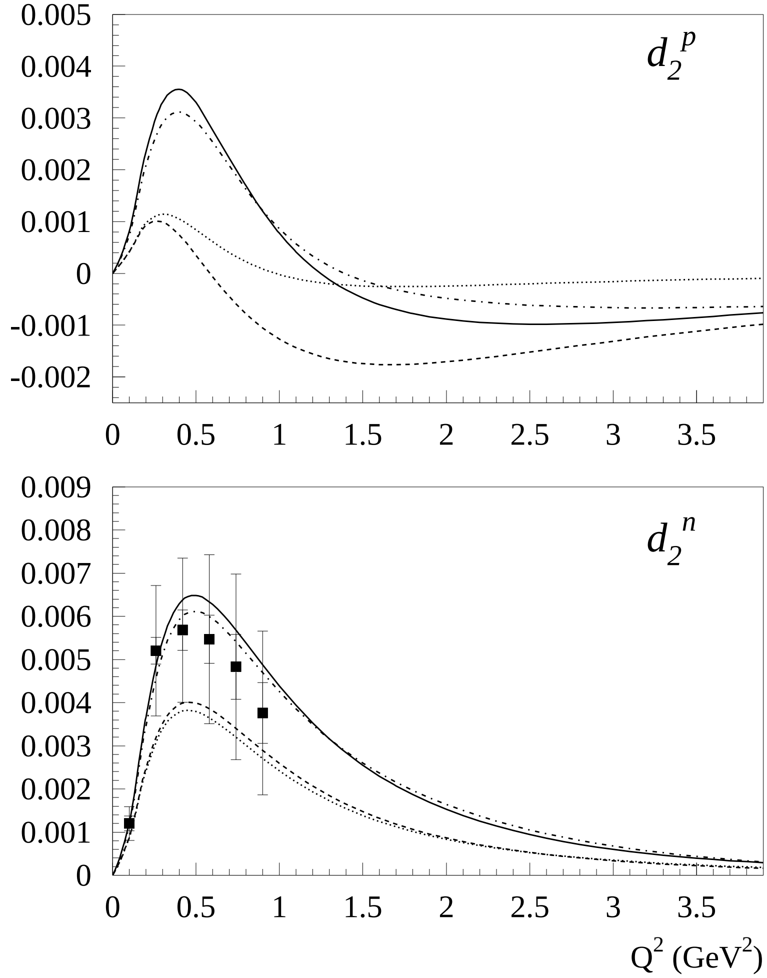

Figure 5: Multipole content of the moment d_2 for proton (upper panel) and neutron (lower panel). The solid curves are the total MAID estimate for the π channel (same as solid curves in Fig. 1). The other curves represent different partial wave contributions. Dashed-dotted curves : results for the sum of s- and p-waves; dashed curves : results for only s-waves; dotted curves : results for s-waves without $S_{11}(1535)$ resonance contribution. Data as in Fig. 1.

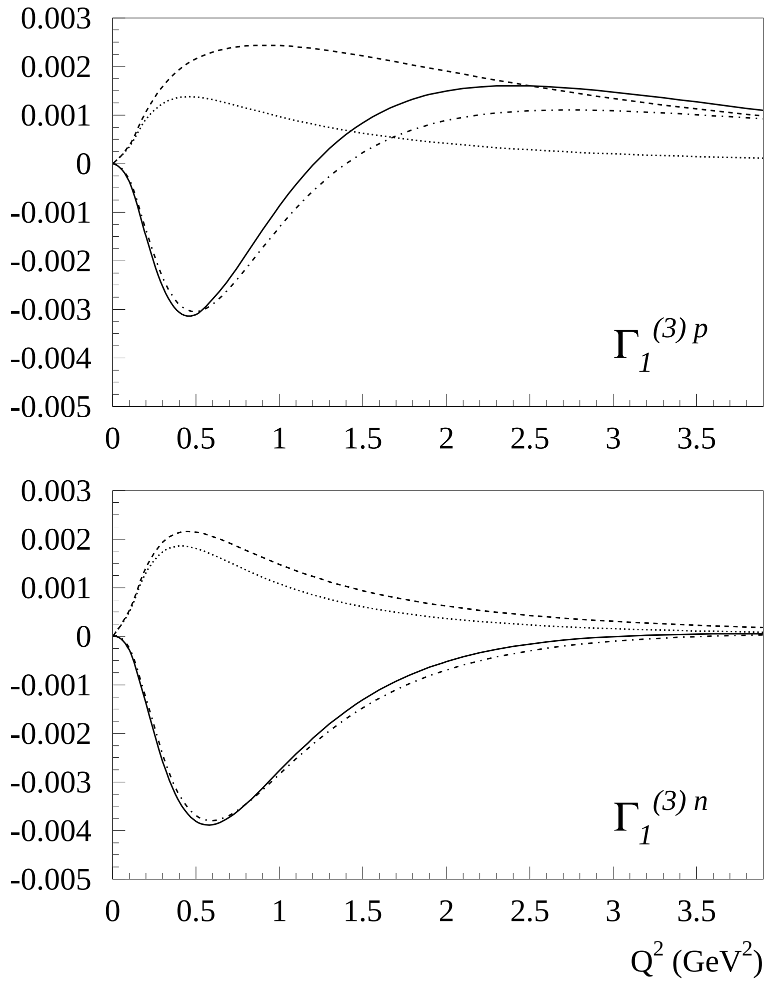

Figure 6: Multipole content of the moment $\Gamma_1^{(3)}$ for proton (upper panel) and neutron (lower panel). The solid curves are the total MAID estimates for the π channel (same as corresponding solid curves in Fig. 2). The other curves represent different partial wave contributions. Dashed-dotted curves : results for the sum of s- and p-waves; dashed curves : results for only s-waves; dotted curves : results for s-waves without $S_{11}(1535)$ resonance contribution.

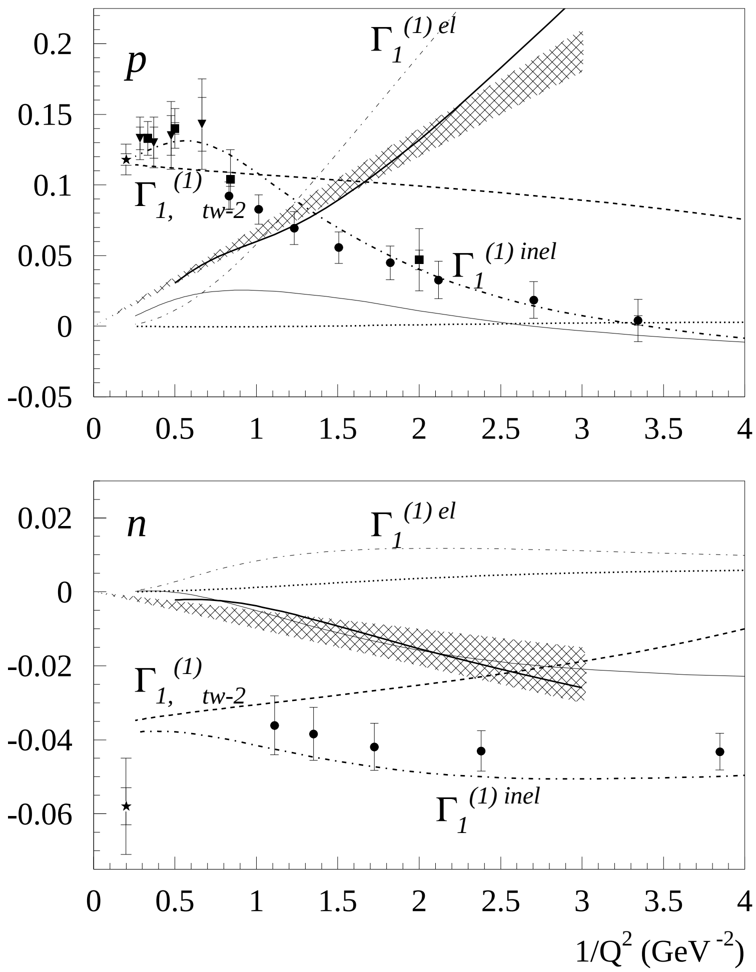

Figure 7: Q^2 dependence of $f_2 \cdot 4M_N^2/(9Q^2)$ (thick solid curves in the shaded bands) for proton (upper panel) and neutron (lower panel) as extracted from Eq. (10). We show separately the elastic $\Gamma_1^{(1)\,el}$ (thin dashed-dotted curves), total inelastic $\Gamma_1^{(1)\,inel}$ (thick dashed-dotted curves), and resonance ($W < 2$ GeV) (thin solid curves) contributions to $\Gamma_1^{(1)}$. We also show the twist-2 part $\Gamma_{1,\,tw-2}^{(1)}$ (dashed curves) and $(a_2 + 4d_2) \cdot M_N^2/(9Q^2)$ (dotted curves) which enter on the *rhs* of Eq. (3) for $\Gamma_1^{(1)}$. The shaded bands are a linear fit to extract f_2 as described in the text. The proton data for $\Gamma_1^{(1)\,inel}$ are from JLab/CLAS [36] (circles), SLAC [46] (diamonds), and HERMES [47] (triangles). The neutron data for $\Gamma_1^{(1)\,inel}$ are from JLab/HallA [37] (circles). The data points at $Q^2 = 5$ GeV^2 (stars) correspond with the global analysis of Ref. [45]. Inner error bars are statistical errors only, outer error bars include systematical errors.